Review Article

BIOMEDICAL Journal of Scientific & Technical Research

ISSN: 2574 -1241

DOI: 10.26717/BJSTR.2022.40.006504

Optical Properties of the Ni Based Aluminide Coating on Inconel

L Castañeda*

Sección de Estudios de Posgrado e Investigación de la Escuela Superior de Medicina, Instituto Politécnico Nacional, Plan de San Luis y Díaz Mirón s/n, Casco de Santo Tomás, Ciudad de México, Mexico

***Corresponding author:** L Castañeda, Sección de Estudios de Posgrado e Investigación de la Escuela Superior de Medicina, Instituto Politécnico Nacional, Plan de San Luis y Díaz Mirón s/n, Casco de Santo Tomás, Ciudad de México, Mexico

ARTICLE INFO

Received: November 05, 2021

Published: January 05, 2022

Citation: L Castañeda. Optical Properties of the Ni Based Aluminide Coating on Inconel. Biomed J Sci & Tech Res 40(5)-2022. BJSTR. MS.ID.006504.

Keywords: Pack Aluminizing; High Temperature Oxidation; Inconel 718; Wear; Hardness

Abbreviations: XRD: X-ray Diffraction; SEM: Scanning Electron Microscope; EDS: Energy Dispersive Spectroscopy

ANNOTATION

Inconel 718 has a wide area of applications in gas turbines, aircraft, turbocharger rotor equipment and so many other applications, including temperatures up to ~700 °C. In this study, Ni based aluminide coating on Inconel 718 alloy was conducted by pack cementation technique. The phase structure and layer coating thickness at different aluminizing temperatures and durations (600 and 700°C for 3 and 5 h) were investigated. This specific substrate material is intended to be coated with aluminum to be used at higher temperatures and it is aimed to be resistant to oxidation thanks to the thin and stable impermeable oxide layer to be formed on its surface. Besides this wear resistance also investigated. SEM/EDS and XRD analysis were used for characterization of the aluminide coatings. The change in layer from the surface to the inside was determined and varied from 8 to 80 μm, this was increased with higher aluminizing temperature and time. 960 HVN hardness value was determined in the coating layer whereas the hardness of the matrix was 240 HV. The wear resistance of Inconel 718 has increased with aluminization. Increased aluminization duration and temperature reduced wear losses. Isothermal oxidation test results at 1000 °C for 5, 25 and 125 h show that the increased aluminization time enabled better oxidation resistance. The formation of porosities below the oxide scale weakened the adherence and durability in low temperature and short time aluminized samples.

Introduction

The alumina film formed on the surface of hard aluminide coatings and when the coating is exposed to high temperature can also prevent oxidation or destruction of the substrate under corrosive environmental conditions [1]. Many different methods can be used for the process of improving surface properties with the aluminide coating method. Some of those are hot dip aluminizing coating [2-5], pack cementation [6,7] physical vapor deposition PVD [8-10] and chemical vapor deposition CVD [11-13] methods are the main ones. From the methods explained above, the pack cementation technique draws attention in terms of not expensive and effective technique besides this with low equipment cost. The pack cementation process can be used to form protective and hard intermetallic coatings on wide variety of alloys. These processes, components of various sizes and different geometries can be coated easily and a homogeneous coating is obtained. Besides, this process is very cheap [14,15]. However, one limitation of the process is that it requires thermal activation to sufficiently generate fast chemical reactions and diffusion kinetics. So, this process is normally conducted at temperatures above 750°C. At these temperatures, it may cause deterioration of the mechanical properties of alloy steels for instance grain coarsening and carbide precipitation. To prevent this degradation, aluminizing should be done at temperatures below 700 °C [7,15-17].

Nowadays the polymeric coatings with functionalized silica nanoparticles has been successfully implemented because of their importance in many technological applications such as hydrophobic/super hydorophobic, to fabricate self-cleaning and antireflective coating on the glass substrate [18]. Additionally, the incorporation of SiO_2–Ag nanofillers into the water-based acrylic coating, had slightly improved adhesion of the coating and had significantly enhanced its abrasion resistance and its thermal stability, for antibacterial activity [19]. Alternatively, the effect of incorporating various nanoparticles such as SiO_2, Zn, Fe_2O_3 on the corrosion resistance of epoxy-coated steel, suggested the beneficial role of nanoparticles in significantly improving the corrosion resistance of the coated steel, with the Fe_2O_3 and halloysite clay nanoparticles being the best [20]. Finally, the SiO_2 nanoparticles play a dual role, as both reinforcer and UV absorber, thus improving effectively both the mechanical properties and the weathering resistance of polyurethane acrylic coatings, offering a durable outdoor application [21].

Alternatively the Inconel 718 is a nickel-based superalloy and has superior properties with the nominal composition of 50–55 wt% of Ni, 17–21 wt % of Cr, 4.8–5.5 wt% of Nb, 2.8–3 wt% of Mo, 0.65–1.15 wt% of Ti, 1 wt% of Co, Al (0.2–0.8 wt%), and Fe (balance) [22,23]. Inconel 718 type material is a very important material group for use in turbine engine discs, blades and drive shafts in the aircraft engine industry thanks to its high strength, high fracture toughness and high corrosion and oxidation resistance. In addition, this alloy contains a wide service temperature range from -253 °C to 760 °C [22]. Despite these superior properties, its tribological properties are relatively poor, and its particularly low hardness and poor wear resistance limit its use in many applications. Therefore, it is technologically important to develop innovative surface modification processes that can increase the wear and oxidation resistance of Inconel 718. To the best our knowledge, few information is available in literature concerning the oxidation and wear resistance properties of Inconel 718 alloy after aluminization coating process at about low temperatures like 600 and 700°C. Therefore, in study microstructure, wear and oxidation properties of Inconel 718 alloy, which was subjected to aluminized process at different temperatures and times, were investigated.

Experimental Details

In this study, Inconel 718 substrate alloy having dimensions of 20 mm× 20 mm× 7 mm were used. The chemical composition (wt%) of Inconel 718 alloy was explained above. Before pack cementation process, all specimens were cleaned with 1000-grit silicon carbide sandpaper and polished with a 3-µm diamond colloidal suspension. Pack aluminizing process, we can see a schematic diagram in Figure 1,it was carried out through immersing the samples into pack powder mixture inside an alumina crucible having a sealed lid. Then the pack was heated in furnace without protective (inert) atmosphere. Aluminide deposition processes were conducted at 600°C and 700°C for 3 and 5 hours respectively. The presence of aluminides formed on the surface was detected by X-ray Diffraction (XRD) analysis. Rigaku X-ray diffractometer (DMAX 2200) with a Cu Kα radiation source of a wavelength of 1.541 Å over a range from 20° to 80° was employed for the phase characterization of coating layer of the test samples. The cross-sectional morphologies of the coated samples were observed and analyzed by a Scanning Electron Microscope (SEM), Model JEOL JSM-6060 from Japan, and equipped with an Energy Dispersive Spectroscopy (EDS). The thickness zone of the aluminide layer was assessed from the element concentration depth profiles measured by SEM-EDS. The micro-hardness values of the specimens were determined by a Vickers diamond pyramid indenter using a load of 25g and dwell time 15s.

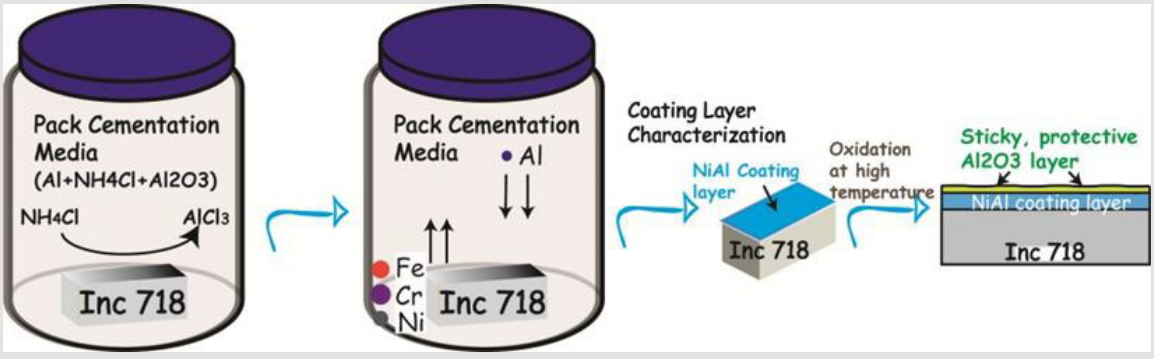

Figure 1: Schematic representation of aluminization process.

The pack aluminizing process can be simply described in four steps [23,24]

a) The stoichiometric ratio that provides a thermodynamic equilibrium state between the activator (NH_4Cl) and the master alloy present in the mixture

b) Gaseous diffusion of metal halides onto the substrate surface present in the can by chemical gradients in gas phase

c) Surface reactions in the substrate to deposit the coating elements and form the vapour phase; and

d) Diffusion of the coating elements at the substrate surface.

Wear tests were performed against a WC ball (6 mm diameter) on the ball-on-disc tribometer wear tester under dry sliding conditions. Tests were carried out under loads of 3, 5 and 8N, at a sliding rate of 5.4 cm/s and at room temperature. The total sliding distance was determined as 100 m and the wear traces were made on a 5 mm linear path. Volume losses were calculated by measuring the width of the tracks from at least 5 different points. The oxidation tests were carried out to Inconel 718 and aluminized samples at 1000 ºC for 5, 25 and 125 h in atmosphere ambient by using an electric furnace (PLF 130/20, Protherm, from Turkey).

Results and Discussion SEM-EDS and XRD Analyses

Unlike other alloys, Inconel 718 contains the γ'' -Ni_3Nb phase [22-26] in its structure. And these Ni_3Nb particles that make this alloy valuable in terms of mechanical properties. However, at about 500°C [27,28] and above temperatures, mechanical properties of this alloy deteriorate from external surface to internal surface of the material under test. Therefore, it is extremely important to make a coating resistant to high temperatures on this alloy [22,23]. We can describe the pack aluminizing process as follows: Firstly, Al atoms pass into the vapour phase with the aid of Cl gases coming from the activator (in our study: NH_4Cl). $AlCl_4$ gaseous diffuses to the substrate surface and reacts with Fe or Ni based alloy forming atomic Al. N H_4Cl then dissociates into NH_3 and HCl at temperature higher than 400 °C [24], as is shown in reaction (1):

$$NH_4Cl_s = NH_{3(g)} + HCl_{(g)}$$

HCl reacts with Al powder and $AlCl_3$ pass into vapor phase:

$$6HCl_{(g)} + 2Al \rightarrow 2AlCl_{3(g)} + 3H_2$$

$AlCl_4$ gaseous diffuses to the substrate surface and reacts with Ni forming atomic Al:

$$3Ni + 2AlCl_{3(g)} \rightarrow 3NiCl_{2(g)} + 2Al$$

The total reaction can be given as follows:

$$3NiCl_2 + 2Al + 3H_2 = Ni_3Al_2 + 6HCl$$

The coating cross-sectional morphology at different aluminizing temperatures and durations are shown in Figure 2. SEM micrographs of the aluminized INC-718 samples revealed that; aluminum deposition realized for all temperatures, and it is observed that the coating thickness increased due to the increasing temperature and time. Besides this it has been shown that diffusion between coating layer and substrate has a good adhesive bonding. The as-coated surfaces can be evaluated very smooth with a metallic appearance. It is also clear that the coating layer was very uniform with a single layer structure as is shown in Figure 2a. The some fracture regions in the outmost layer were probably caused by cutting and grinding stage of the metallographic sample preparation and also indicating the brittle nature of fragile aluminide (inter metallic) material characteristic. Another result is that due to the increasing process temperature, the interface has become roughly. EDX analysis of the points given in Figure 2 is given in Table 1. As it seen from SEM-Map elemental analyses in Figure 3, aluminum were deposited intensively in the coating layer. In addition, that, Cr and Ni are seen in the top layer of the coating.

Table 1: EDS results of layers in Figure 2.

Phases 600°C-34						
Al	**Ni**	**Fe**	**Cr**	**Nb**	**Mo**	**Ti**
72.538	14.834	6.067	4.951	0.408	0.790	0.412
258.274	27.350	6.599	5.451	0.794	1.049	0.483
Phases 600°C -5h						
Al	**Ni**	**Fe**	**Cr**	**Nb**	**Mo**	**Ti**
79.096	12.429	3.946	3.556	0.198	0.546	0.229
276.056	11.727	5.328	5.39	0.684	0.385	0.423

Phases 700°C-3h						
Al	**Ni**	**Fe**	**Cr**	**Nb**	**Mo**	**Ti**
79.209	11.997	6.082	1.696	0.365	0.350	0.302
277.100	14.261	5.072	2.812	0.332	0.392	0.032
Phases 700°C-5h						
Al	**Ni**	**Fe**	**Cr**	**Nb**	**Mo**	**Ti**
77.268	13.394	4.565	3.793	0.517	0.291	0.006
276.520	11.645	5.060	5.437	0.645	0.352	0.340

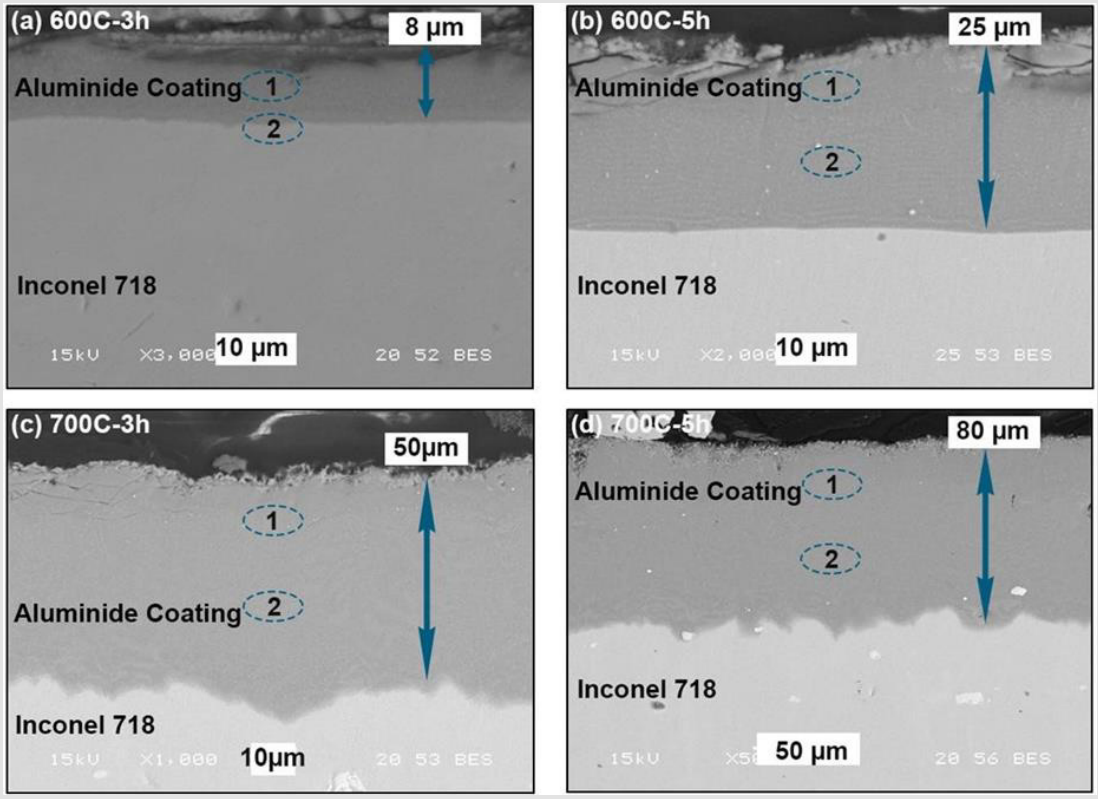

Figure 2: SEM-EDS Analyses of cross sectional morphology of aluminide coated Inconel 718 sample
a) 600°C-3h
b) 600°C-5h
c) 700°C-3h
d) 700°C-5h.

The XRD patterns are shown in Figure 4, we can identify that the top layer includes mainly of Al_3Ni_2 and Al_3Ni with a small quantity of Al-Cr inter metallics ($Al_{86}Cr_{14}$). Looking at XRD analyses results measured from the as-coated surface, it was detected; when the major phase in the surface layer formed at 700°C-5h was $NiAl_3$. According to the Ni–Al phase diagram, the outmost layer formed on the surface is expected to be Al rich $NiAl_3$ phase [16]. However, for the process at 600°C-3h shows that the coating layer has Ni rich aluminide phase such as Ni_3Al. This outcome can be resulted from due to the thin coating layer (~8µm) and thus the analysis obtained from nickel rich region substrate. Wang, et al. [16] obtained an outer Ni_2Al_3 layer and an inner Ni layer for a sample aluminized at 650 °C for 4 h in a pack 6Al–92Al2O_3–2$AlCl_3$ (wt.%) Ni based superalloy according to XRD analyses measured from the surface.

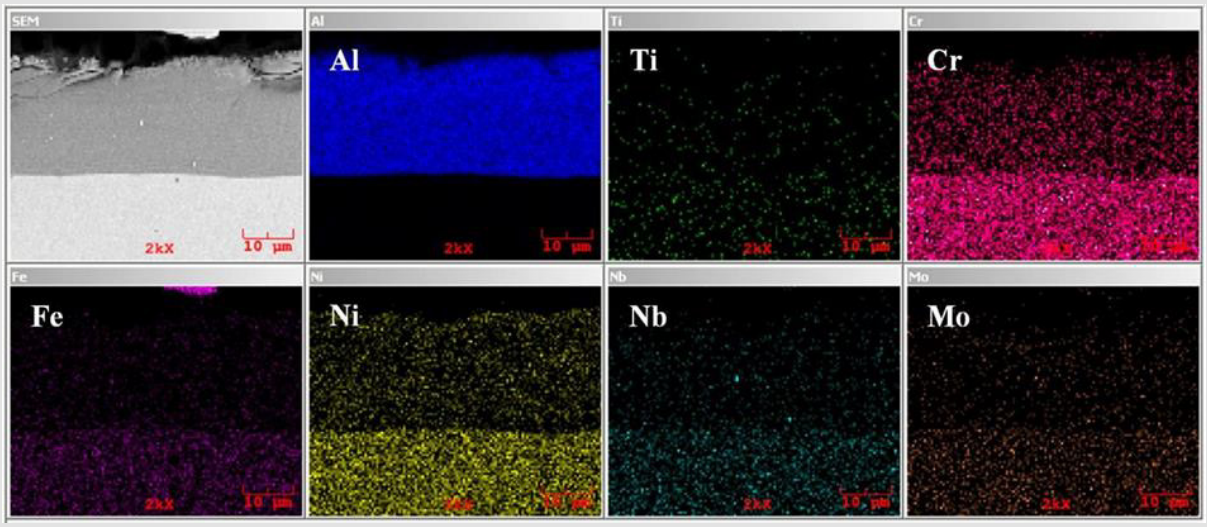

Figure 3: SEM-MAP Analyses of aluminized Inconel 718 at 600°C-5h.

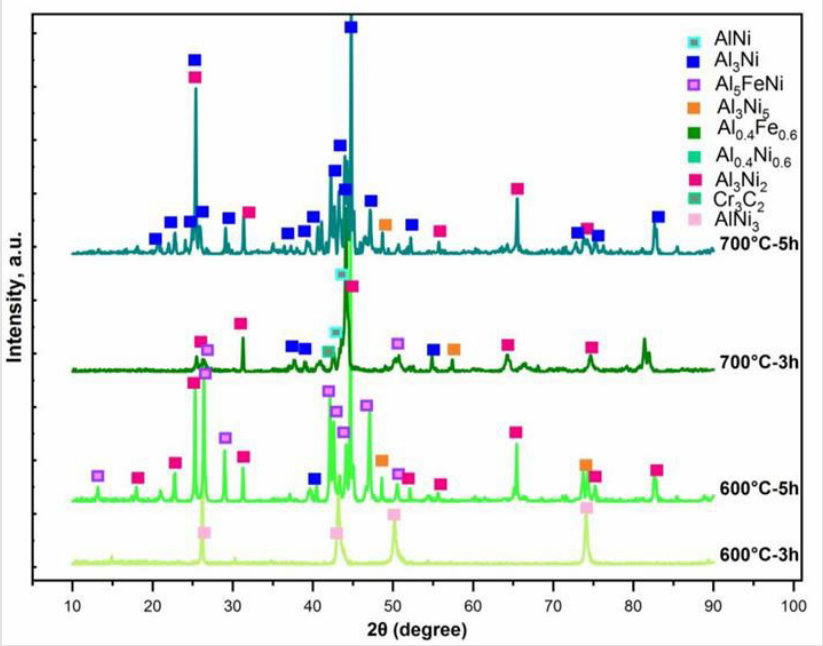

Figure 4: XRD pattern of Al coated Inconel 718 sample.

Hardness

Micro hardness measurements were carried out from the surface to interior along a line to characterize variation of hardness in aluminides layer, transition zone if any and matrix, and the results were given in Figure 5. The hardness of aluminide layer was found to having maximum 900 HV for 700 °C 6h aluminizing process, whereas the hardness of substrate was 270 HV and it was also shown that the area has averagely 500–700 HV, which is in the transition region for Inconel 718 substrate. This hardness increment can be attributed to different aluminide formation vicinity of the top region [17]. Besides this, the coating obtained with increasing temperature and time; being hard, tight and non-porous. This is another important factor in increasing its hardness. When the micro hardness values are examined, the hardness value on the surface of the samples increased with increasing process temperature and duration. The increase in temperature resulted in a denser layer and the expected high hardness of the intermetallic phase was achieved [7,17].

Wear Behavior

We clearly see that Figure 6a shows the volume loss values of the samples which were subjected to dry sliding tests under 3, 5 and 8 N loads after being aluminized at different temperatures and times. First of all, it is seen from the graph that the untreated Inconel 718 sample had the highest volume loss at all loads. It is possible to associate this reason primarily with its low hardness. Because when Figure 5 is carefully examined, an increase of up to 3 times has been observed in the hardness of the treated materials. When the hardness values of the samples were examined, 900 HV was reached for the sample coated at 700 °C 5h. Hardness can be defined as the resistance of an object to another object trying to sink into it. The increase in hardness caused the abrasive ball to sink less into the sample, thus causing less wear loss. When the volume losses of the samples are interpreted according to the aluminizing temperature and time, it is seen that the increasing temperature and the duration reduce the volume losses. Considering the situation with the microstructure, the increase in both the temperature and the duration caused the thickness of the hard coating layer formed on the Inconel 718 to increase. While the coating thickness of the sample treated at 600 °C 3h was approximately 8 µm, at 700 °C 5h this value became 80 µm with a 10-fold increase. This means that the material coming from below instead of the material removed during wear has high hardness. The thick coating provides high resistance to wear. This situation was seen in the sample aluminized for 3 h at 600 °C. With the increase in load during wear, the coating layer was completely removed and caused the wear loss to increase rapidly.

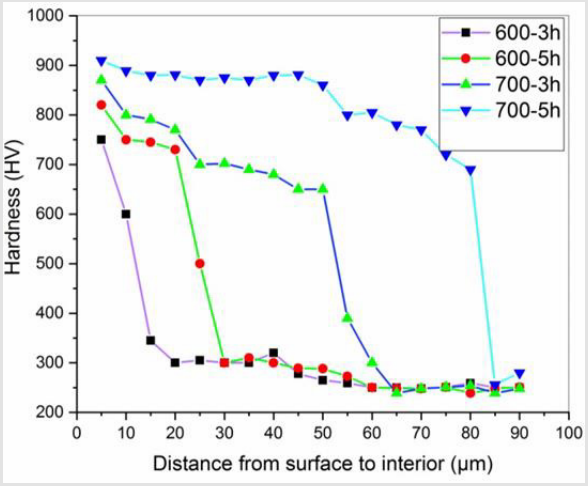

Figure 5: Hardness graphs from surface to interior.

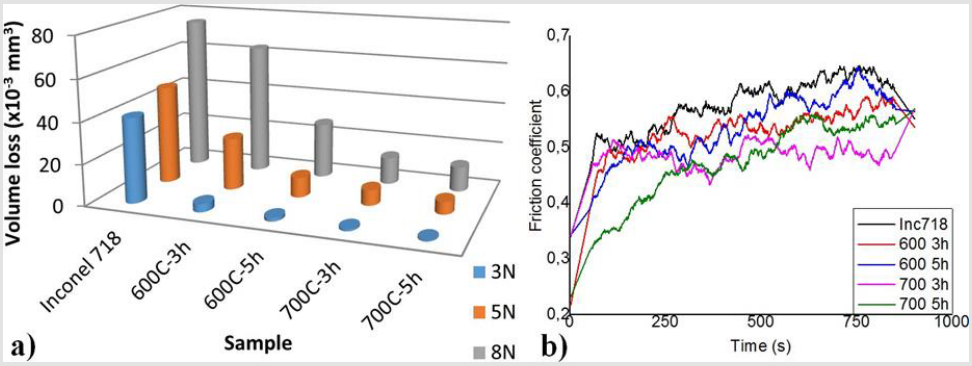

Figure 6:
a) Volume loss values of substrate and coatings
b) Friction coefficient curves for substrate and coatings in tests performed under 8N load.

The friction coefficient (COF) values that occurred during the wear tests of the samples under 8 N load are given in Figure 6. If we evaluate the samples in general terms of COF values, it can be said that there is a tendency to decrease in COF values with increasing hardness. In most samples, stabilization due to oxidation occurred after 100-150s. If the COF values of the samples under 8N load are

DOI: 10.26717/BJSTR.2022.40.006504

examined, it is understood that the highest COF value was in the Inconel 718 untreated sample. A sudden rise in the first 100s can be considered as cleaning the roughness. The stagnation observed in the next 100 s period can be explained as the plastering of the wastes resulting from the breaking of the roughness on the surface under the effect of the load and then oxidation as a result of relative motion. The subsequent fluctuations can be explained by the rupture and regeneration of the oxide layer formed on the surface over time. There was a tendency for the friction coefficient to decrease due to the increase in the coated sample hardness. Generally, similar trends are present for all coated samples. The fluctuations seen in the substrate material were also seen in the coated samples for the same reasons. Particularly in samples with high coating temperature and time, the rapid increase seen in COF at the beginning and stabilized more rapidly afterwards. The high affinity of Al to oxygen is known. For this reason, oxidation occurred faster in the coated samples during wear. It has been shown in many studies that these oxides formed during wear reduce the friction coefficient and thus wear losses. Another reason for the low friction coefficient of the Al coated samples can be shown as this situation.

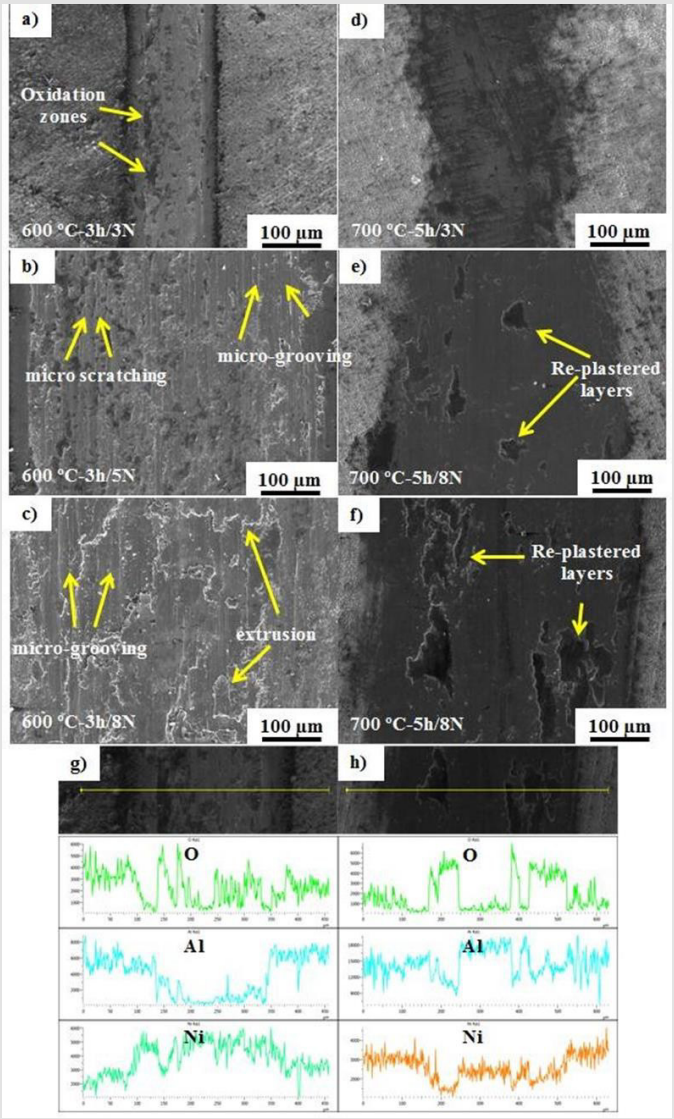

Figure 7: SEM and EDX analysis of the worn surfaces:
a) 600 °C-3h tested under 3N
b) 600 °C-3h tested under 5N
c) 600 °C-3h tested under 8N
d) 700 °C-5h tested under 3N
e) 700 °C-5h tested under 5N
f) 700 °C-5h tested under 8N
g) 600 °C-3h tested under 3N
h) 700 °C-5h tested under 8N.

SEM worn surface images of the samples, which were subjected to aluminizing at 600 °C for 3h and tested under 3,5 and 8N loads, are given in Figures 7a-7c. It can be seen in Figures 7d-7f that the coating layer completely is not destroyed, but there are partial oxidation zones on the surface. When the wear surfaces of the same sample occurring under 5 and 8 N loads are examined, it is seen that the coating layer has been completely removed and the substrate material has been reached. It is possible to understand this situation both from the wear trace and EDX analysis, as is shown in Figure 7g. In the test performed below 5N, there are micro scratching and micro-grooving wear mechanisms in the direction of wear. In the sample tested at 8N, extrusion type wear mechanism was determined in addition to micro grooving. In EDX analysis, it can be seen that the amount of Al decreases significantly in the middle parts of the wear trace. SEM wear trace micrographs of the sample coated at 700 °C for 5h are given in the Figures 7d-7f.

It can be said that the wear mechanism of the sample changes completely with the change of the coating process duration and temperature. This can be attributed to the high hardness and coating thickness. Samples with high hardness and coating thickness showed higher resistance to the abrasive tip reaching the substrate surface and the wear mechanisms occurred only in the coating layer. In the samples tested under 5 and 8 N loads, the wear particles separated from the surface over time were squeezed between the abrasive tip and the bottom surface and re-plastered on the surface. This situation was not observed after the test under 3 N load, probably due to the low load. We can associate this with the effect of the compression load that occurs between the surfaces with increasing load. The particles removed with the increased load can be re-plastered rather than thrown out of the system. EDX analysis of the wear trace of the sample is given in Figure 7h. It is possible to understand from the high percentage of Al in the center of the wear trace that the coating layer was not be overcome even in the test performed under 8N load.

Oxidation Behavior

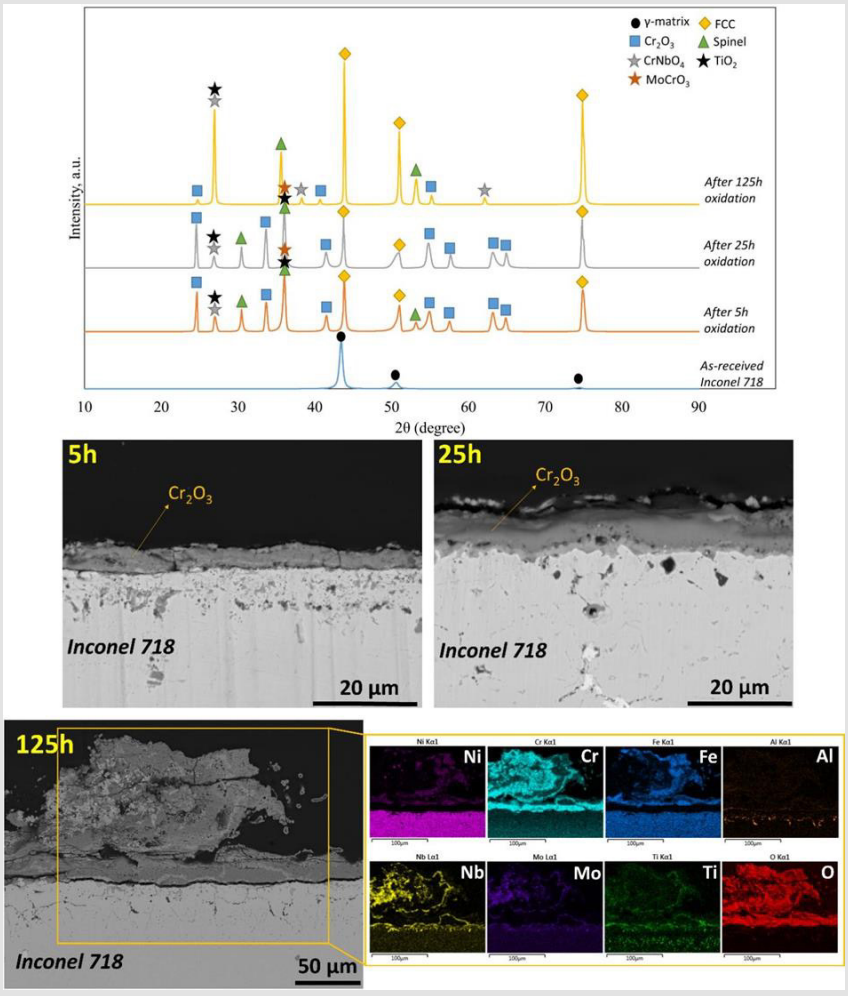

Figure 8: XRD patterns and SEM images belonging to Inconel 718 after oxidation tests.

 DOI: 10.26717/BJSTR.2022.40.006504

We can also see that Figure 8 shows the XRD and SEM images of Inconel 718 after oxidation tests at 1000 °C for 5, 25 and 125 h. At the first oxidation test, oxide thickness shows a dramatic increase compared against the 25 h oxidation test. The obtained XRD analysis result show that Cr_2O_3, spinel and $CrNbO_4$ oxides formed on the surface. It can be said that Cr_2O_3 is more dominant for this oxidation stage. After 25h oxidation, the same tendency is seen in terms of formed oxide phases and there is no significant increase in oxide thickness. However, after 125 h oxidation, $CrNbO_4$ oxide has stronger intensity among the formed oxides. It can be also seen in the SEM image. The oxide layer delaminated and reached a high thickness in some regions at the last oxidation stage. According to elemental mapping analysis, darker grey colors represent Cr_2O_3 and spinel whereas others represent $CrNbO_4$, $MoCrO_3$, and TiO_2 oxides. The inner oxide layer dominantly composed of Cr_2O_3 layer while the upper oxide layer consists of mixed oxides.

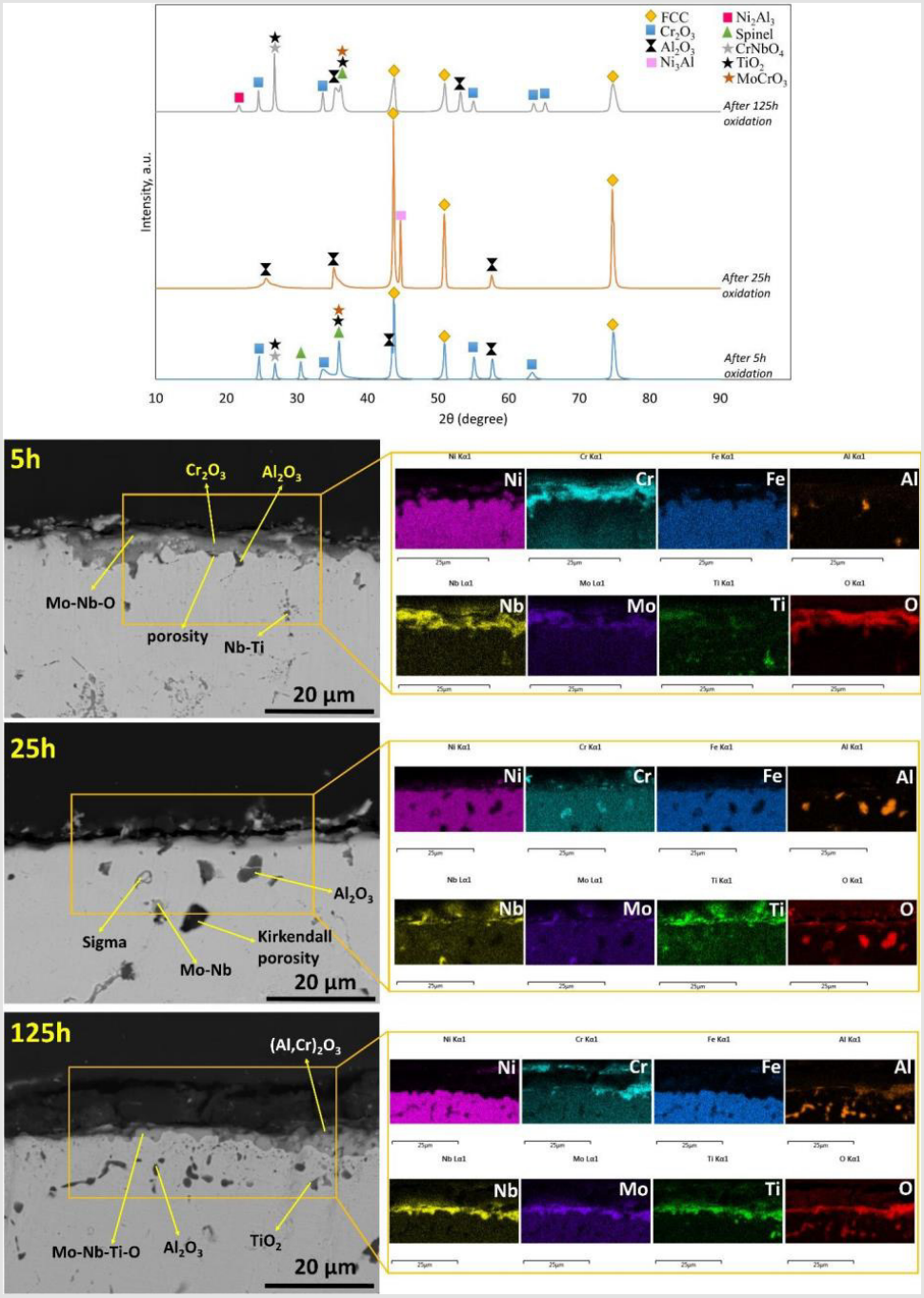

Figure 9: XRD patterns and SEM images belonging to 600 °C-3h after oxidation tests.

This also proves that oxides except for Cr_2O_3 have high growth rate and generated higher thermal stress on the oxide scale. Additionally, Cr concentration was significantly decreased in Inconel 718 and accordingly, it is understood that other elements diffuse toward the above Cr_2O_3layer and formed spinel and mixed oxides on the surface. After oxidation tests, γ-matrix phases rich in Fe-Ni-Cr transformed to FCC phases rich in Fe- Ni depending on depleting Cr concentration. In the matrix, Ti, Nb and Mo oxidized as inner while Al oxidized at grain boundaries due to its lower melting. Phases rich in Al such as Ni_3Al, Ni_2Al_3 and AlNi enable to alumina formation on the oxide scale during the oxidation. From this perspective, aluminide coatings widely performed on the Ni-based superalloys to get alumina-former phases [29]. In Figure 9, XRD patterns and SEM images of aluminized Inconel 718 at 600 °C for 3 h (600 ºC-3h) were given after oxidation tests at 1000 °C for 5, 25 and 125 h. 600C-3h sample had about 8 µm thickness after the aluminizing process. The obtained coating thickness is very low and thus, it did not provide a continuous alumina scale on the surface after oxidation tests. The obtained XRD peaks in 5h oxidation test shows that matrix phases composed of FCC phases rich in Fe and Ni while spinel, Cr_2O_3, $CrNbO_4$, $MoCrO_3$, TiO_2 and Al_2O_3 formed as oxide phases. It is understood that Al rich phases rapidly depleted and, the alumina layer formed was delaminated from the base material. According to SEM image after 5 hour oxidation, Cr_2O_3, Nb and Mo rich oxides and inner Al_2O_3 can be seen.

In 5h oxidation stage, porosity could be seen below the oxide scale. The porosity formation weakens the durability and adherence of oxide scale, that's why the delamination can occur on the oxide scale. After 25 h oxidation test, the formed oxide layer delaminated from the base material and, embedded Al_2O_3 and porosity formation are seen. This porosity can be called Kirkendall porosity due to difference in phases, concentrations and diffusion coefficients [30]. The thinner coating layer may cause porosity formations in interdiffusion regions where they are near to the surface. The matrix phase, Ni_3Al and some Al_2O_3 peaks were found on the surface according to XRD analysis. When looking at the mapping colors, it can be seen that Al was almost depleted as well as decreasing of Cr concentration. In the initial stage of oxidation, Al_2O_3 can expose to phase transitions such as γ, δ, θ and α- Al_2O_3. The thermodynamically stable phase is α- Al_2O_3 among these phases [31]. It is known that the phase transition between θ and α- Al_2O_3 occurs at a temperature range 950-1050 ºC [32]. Other polymorphs except for α- Al_2O_3 show a fast growth that means the phase transitions in Al_2O_3cause the rapid depletion of Al-rich phases, as well. As a result, phase transformations are seen in both coating and oxide layers. The possible phase transformations of both Al_2O_3 and Ni-Al phases can lead to stress generation in the oxide scale. Furthermore, Ni-Al phases are high thermal expansion compared to γ and FCC phases [33]. As a result of all, the formed oxide layer spalled on the surface.

After 125 h oxidation, the oxide scale is not seen due to spallation similar to 25h oxidation stage. Mo-Nb- Ti rich oxides were formed on the surface and, Al oxidized as inner. According to XRD analysis, $CrNbO_4$ phase is more dominant among the formed oxides. In some regions, not spalled Cr_2O_3 and Al_2O_3 scales can be seen in the SEM images. The obtained results show that 600 ºC-3h exhibited a breakaway oxidation behavior. This can be attributed that the formed total coating thickness is not sufficient to form a continuous and protective alumina layer. Additionally, we can see that Figure 10 represents XRD analysis results and SEM images of aluminized Inconel 718 at 600°C for 5 h (600C-5h). When looking at the SEM image after 5h oxidation test, compact and continuous alumina formation are seen. The alumina layer includes some porosities and, subsurface regions also have small porosities. Al concentration is very low according to mapping analysis. The matrix composed predominantly of Ni-Cr-Fe as well as Nb, Mo and Ti. It is not seen precipitate or distinct phase formation. However, Fe, Ni-rich FCC phase, NiAl, Ni_2Al_3 phases were obtained according to XRD analysis while predominant alumina phase and Cr_2O_3 were detected as oxide phases. Besides, the oxide thickness is slightly high. High thickness can be also associated with the alumina transition phases. In the literature, Ni_3Al can be effective in the formation of γ-Al_2O_3 while the formation of θ- Al_2O_3 is more predominant in NiAl [34]. The presence of Ni_2Al_3 or $NiAl_3$ phases can lead to a porous oxide layer as indicated in the literature [35]. This result agrees with our result as observed SEM image and XRD patterns.

After 25 h oxidation test, the formed oxide layer dominantly composed of alumina according to both XRD and mapping analysis. However, the oxide scale delaminated from the base material. Also, a minor number of base materials stick to the oxide scale broke off from the surface. This is related to the porosities which are formed below the oxide scale and this led to a decrease in the durability and adherence of the oxide layer. In addition, after the delamination, mixed oxide formation traces are visible on the base material. This shows that after the depletion of Al, other elements were oxidized in porosities and can lead to an increase in the stress generations in these regions. After 125 h oxidation test, the oxide layer has a compact and continuous alumina layer. Cr_2O_3, $CrNbO_4$ and TiO_2 peaks were found according to XRD analysis. These phases could be remained from the initial oxidation stage or formed due to the depletion of Al. The delamination was not observed in the oxide scale, interestingly. That may be related to (Al, Ti) N phase formations that are seen below the oxide scale. N penetration due to the consumption of O may lead to formation of (Al, Ti) N phases [36,37]. The formation of these nitrides is in good agreement with the obtained XRD data. The formed nitride also provides the lowering in CTE of base material. CTE of TiN and AlN is about 2.3 and 5.7×10-6 K, respectively [38]. It is thought that the presence of these phases with low CTE may generate lower stress at the interface. Therefore, the oxide layer may not delaminate as occurred in 25 h-oxidation tests.

DOI: 10.26717/BJSTR.2022.40.006504

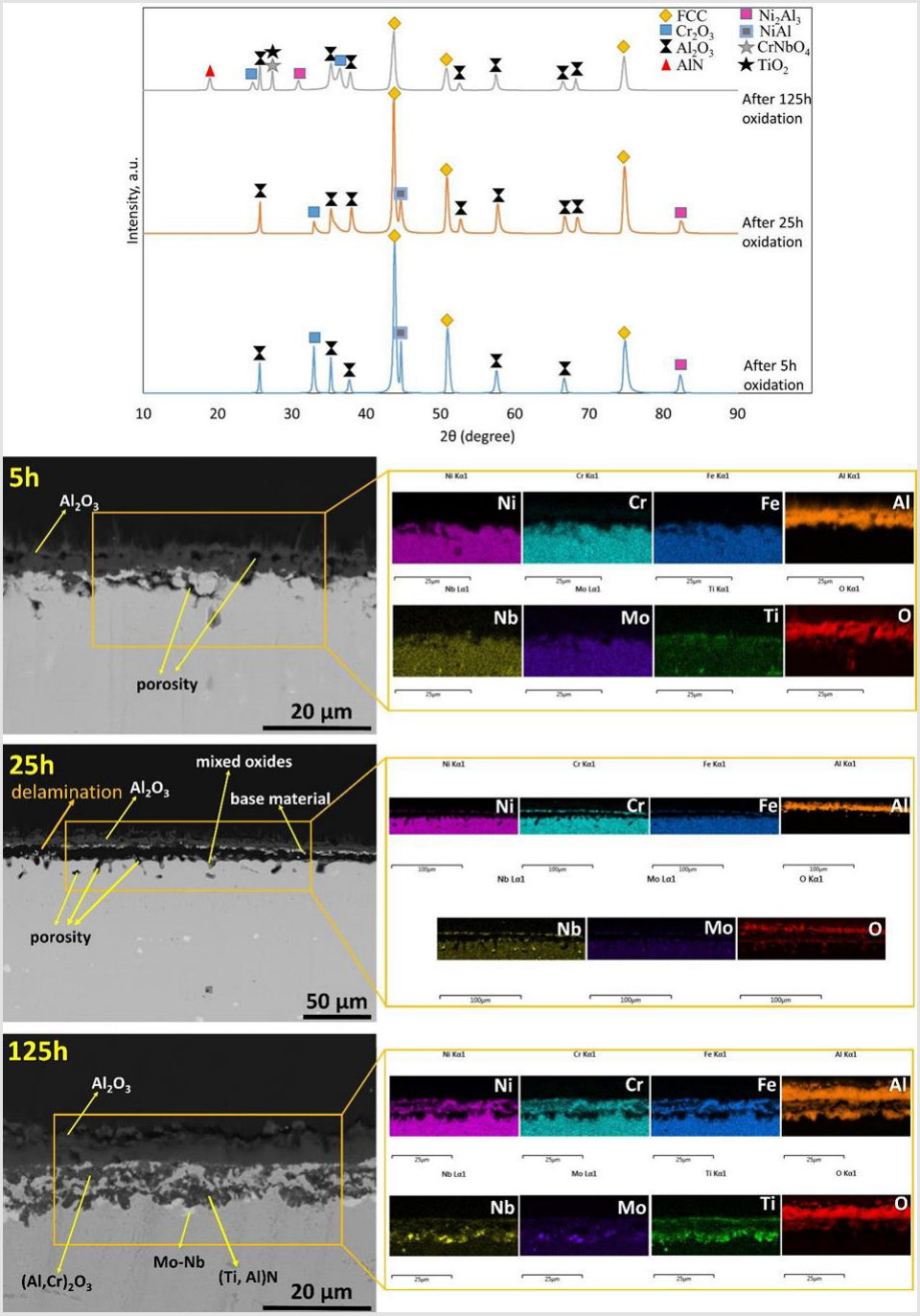

Figure 10: XRD patterns and SEM images belonging to 600 °C-5h after oxidation tests.

The SEM images and XRD patterns belonging to aluminized Inconel 718 at 700 °C for 3 h are given in Figure 11. After 5 h oxidation stage, the total coating thickness thickened more with the high temperature effect. The formed oxide layer predominantly composed of alumina while the matrix phase consists of NiAl and Ni_2Al_3. The Cr-rich precipitates formed in the Interdiffusion Zone (IDZ) and, cavity formation was not observed in these regions. Ni rich- Ni_3Al phases were detected above the IDZ zone according to coincided element colors in mapping analysis. The upper layer is composed of Al-rich intermetallic as seen in mapping image and XRD data. The presence of NiAl and Ni_2Al_3 phases lead to Kirkendall porosities on the top regions due to the intrinsic diffusivity difference of Al and Ni in Ni_2Al_3 [35]. Al- poor zones increasing the Cr solubility can form cavities [34]. The reason of the local delamination in the oxide scale could attribute to the formation of these cavities. After 25h oxidation, Cr rich sigma phases are seen.

In the SEM image, brighter gray colors represent sigma phases while the brightest colors show Mo-Nb-Ti-rich precipitates. The presence of Cr precipitates support transition from θ to α-Al_2O_3. In addition, the formation of Cr_2O_3 nuclei enables the nucleation of α- Al_2O_3, as well [39]. Cr_2O_3 phases (as seen in XRD peaks) and the presence of sigma phases enabled the continuous and stable Al2O3 phase formation on the surface. In this oxidation stage, the porosity formation may be lower than other periods due to the formed precipitates and complete transformation of the Ni-Al phases. Additionally, it was indicated that the presence of sigma phases act as a diffusion barrier in Inconel 718 [40]. This may prevent the porosity formation by contributing to slower diffusion of elements. However, after 125 h oxidation stage, the crack formations in the substrate and oxide layer are seen. This probably related to the stress of high growth rate and TEC mismatch. The extents of sigma precipitate phases increased whereas the distribution of Mo-Nb-Ti-rich precipitates decreased after 125 h oxidation. This phase variation might occur crack formations leading to the volume change. Nonetheless, the oxide scale did not delaminate. The oxide layer predominantly consisted of alumina layer.

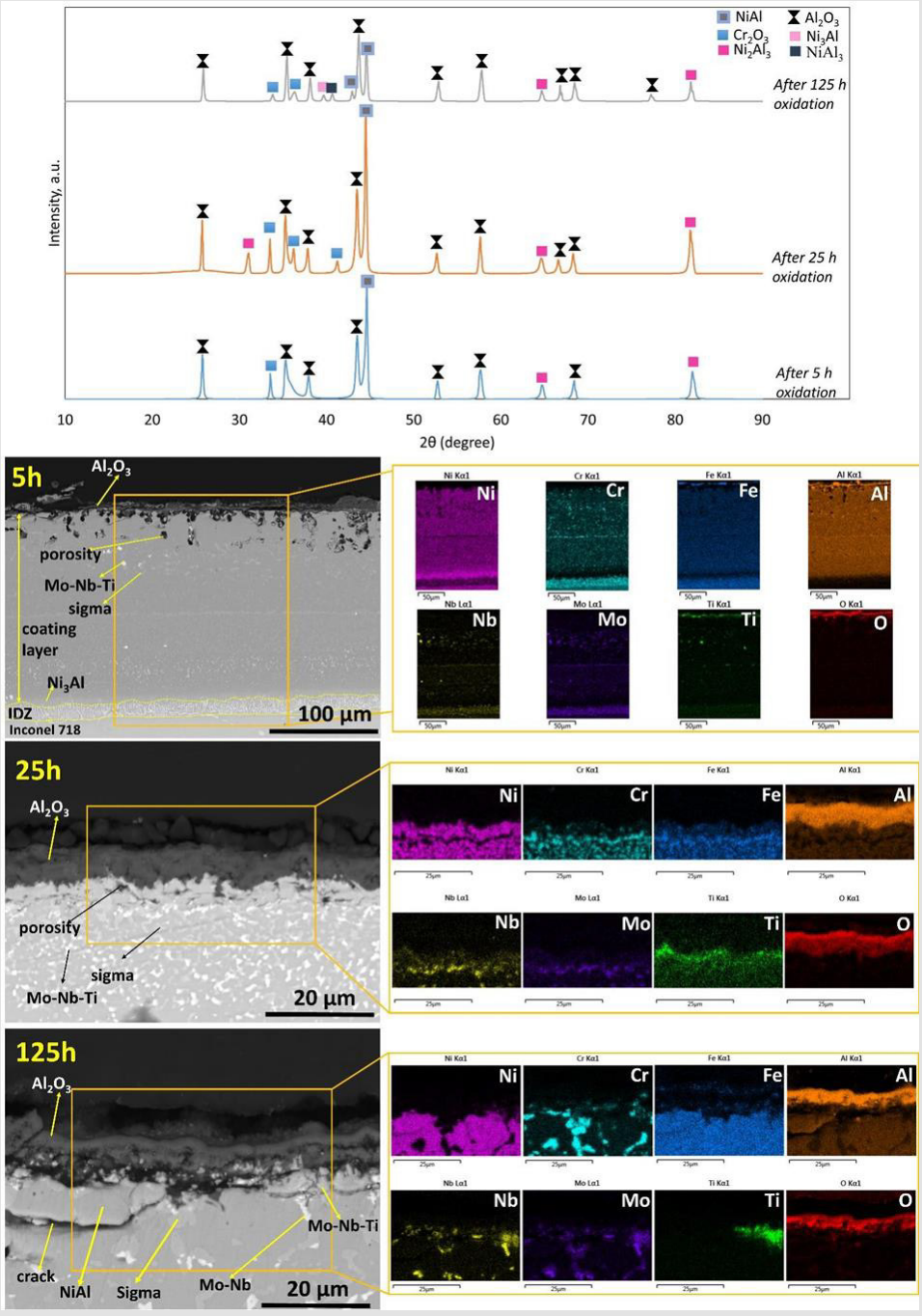

Figure 11: XRD patterns and SEM images belonging to 700 ºC-3h after oxidation tests.

DOI: 10.26717/BJSTR.2022.40.006504

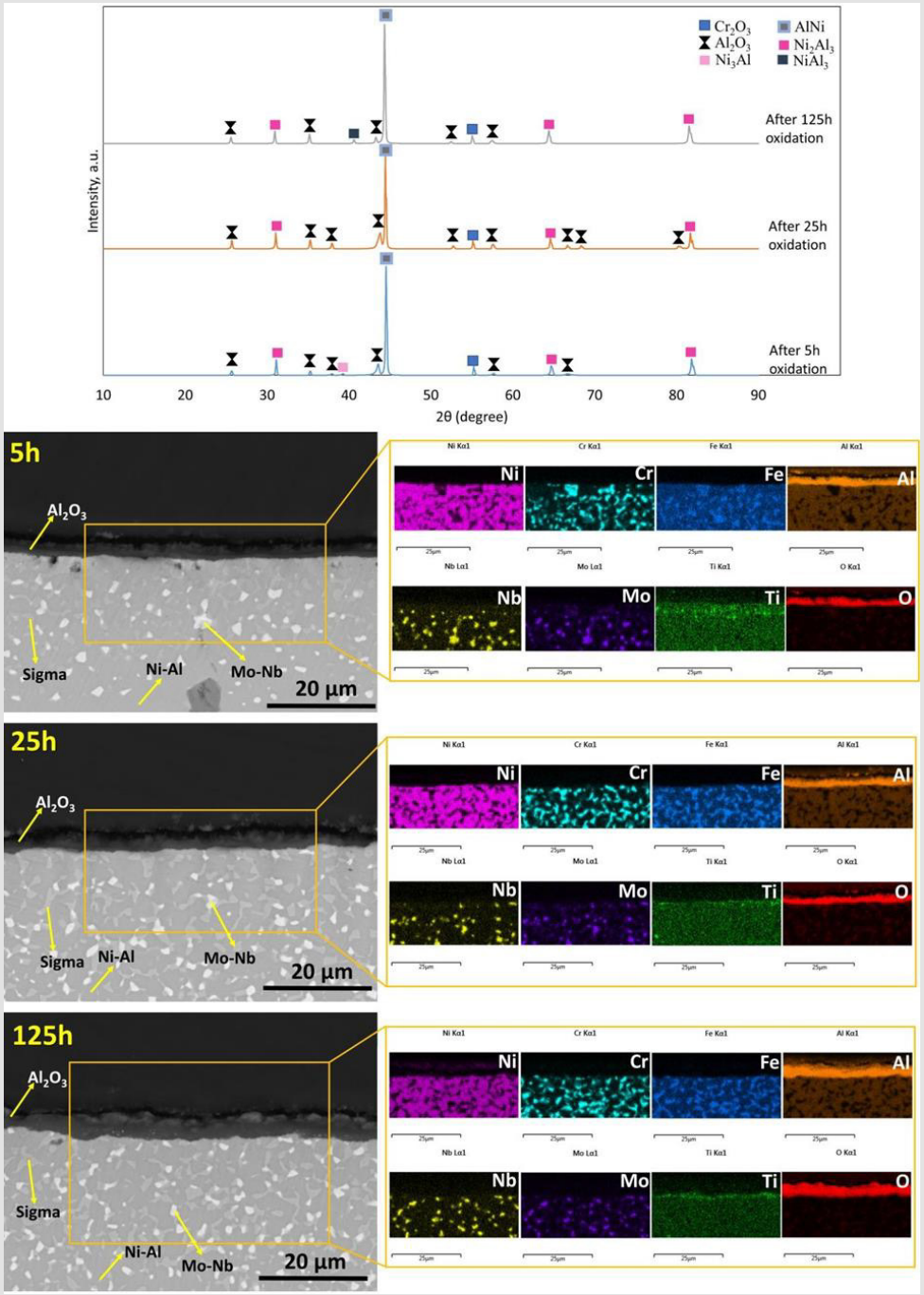

Figure 12: XRD patterns and SEM images belonging to 700 ºC-5h after oxidation tests.

After the isothermal oxidation tests, SEM, mapping and XRD analysis results of aluminized Inconel 718 at 700 °C for 5h (700ºC-5h) are shown in Figure 12. In all oxidation stage, compact, homogenous and continuous alumina scale as well as Cr_2O_3 was obtained in 700 ºC- 5h. The highest increase in oxide thickness was seen in the first stage of oxidation. The presence of various Ni-Al phases was detected according to XRD analysis. However, the most dominant phase is the stable NiAl phase. Besides, sigma phases rich in Cr and Nb-Mo-rich phases could be seen in SEM and elemental mapping images. After 25 h oxidation, the oxide scale composing of alumina shows a slight increase in thickness. According to obtained SEM and mapping analysis, the same matrix phases as 5 h oxidized sample are seen. The highest oxide thickness was obtained after 125 h oxidation test. The similar phase distributions in terms of both matrix and oxide phases were seen at the end of the oxidation, as well. Porosity or cavity formations were not seen as the other aluminized samples. The main difference in this sample, the matrix phase distribution was uniform in each oxidation stage. It

is thought that the presence of other phases may be effective in the oxide formation with lower thickness. It is thought that longer aluminization time and temperature provided to obtain more stable coating layer since free Al and Al in Ni-Al phases have different diffusion speed. Therefore, porosity formation can be seen in the coating layer.

Koech et al. applied to a hot-dip aluminizing on Inconel 718 [41]. The free Al was formed on the top coating layer while Al3Ni phases formed below this layer. This formation led to big Kirkendall porosity formation after the oxidation test at 750 °C for 90h. This result shows that the coating layer did not find an enough time to form a stable coating layer as process time is short in hot-dip aluminizing process. In our previous study [15], the pack aluminization process was subjected to ESR steel at 700 °C for 2, 4 and 6 h. The best oxidation resistance agrees with the current study in terms of longer aluminization time. We can see that Figure 13 shows the graph of the variation in oxide scale thickness depending on oxidation time. In the graph, Inconel 718 and 600 ºC-3h samples were not given due to spallation and breakaway oxidation trend. The obtained graph shows that almost the same oxide growth tendency was observed in 600 ºC-5h and 700 ºC-3h while 700 ºC-5h exhibits slower growth. Depending on the obtained thickness, parabolic growth was seen and the oxide growth rate was calculated based on the indicated formula below.

$$X^2 = k_p.t + C$$

where x is oxide thickness (μm), k_p is parabolic oxide growth rate ($\mu m \cdot h^{-1}$), t is time and C is constant. The slope of the graph drawn using the above formula found the k_p values. The calculated k_p values are 0.115, 0.117 and 0.066 μm·h-1, respectively. The highest increase was obtained in the initial oxidation stage for all samples. After the initial oxidation period, oxide growth tends to increase decreasing. According to obtained k_p values, the slowest and reliable oxide growth was seen in 700 ºC-5h whereas the others were near to each other in terms of k_p value.

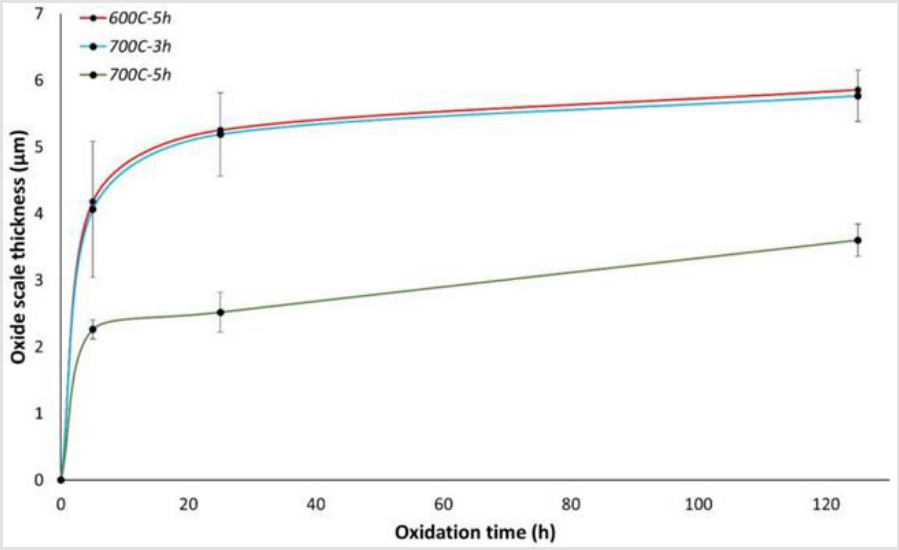

Figure 13: Oxide growth graph of 600C-5h, 700C-3h and 700C-5h.

Conclusion

In this study, the effect of low temperature aluminizing process on microstructure, wear and oxidation properties of Inconel 718 was investigated. For this purpose, aluminizing process was applied to the INC718 substrate at temperatures of 600 and 700°C for 3 and 5 hours. After the production of samples, wear and oxidation tests were carried out on the samples and obtained results were listed below.

a) Low temperatures such as 600°C -3 hours can be evaluated as initial temperatures for aluminide coating formation. According to XRD analyses, while the Ni3Al phase was obtained at 700°C, the $NiAl_3$ phase of the thin coating layer formed at a lower temperature (600°C) was determined. Characterization of the coating layer can be described fully dense and uniform on the Inconel 718 substrate.

b) Time and temperature has led to positive effect on the coating layer and varied from 8μm to 80 μm after aluminizing process.

c) By hardness measurements from the surface to the substrate, it has been determined that, aluminide coated zone has 960 HV hardness value top of the layer at 700°C whereas hardness of matrix is about 250HV.

d) The aluminizing process contributed positively to the wear resistance of Inconel 718, regardless of temperature and time. However, with the increasing aluminizing duration and temperature, wear losses decreased even more.

e) After the oxidation tests, Inconel 718 was severely affected and formed a thick oxide layer. Delamination and crack formations were observed during oxidation tests. In 600ºC-3h, breakaway oxidation was seen. The lower coating layer did not provide a continuous alumina scale on the surface.

f) 600 ºC-5h and 700 ºC-3h show the similar oxide growth. However, delamination was seen in 600ºC-5h after 25 h oxidation test. The best oxidation performance was obtained in 700ºC-5h. The fully dense and continuous alumina layer formed on the surface. The presence of Cr rich sigma phases and Mo-Nb precipitates provided a positive contribution on the oxidation behavior of aluminized samples.

Acknowledgement

The authors gratefully acknowledge the financial support from the Escuela Superior de Medicina, Instituto Politécnico Nacional, through Project no. 20210385.

References

1. J Dong, Y Sun, F He (2019) Formation mechanism of multilayer aluminide coating on 316L stainless steel by low-temperature pack cementation. Surface and Coatings Technology 375: 833-838.
2. S Han, H Li, S Wang, L Jiang, X Liu (2010) Influence of silicon on hot-dipaluminizing process and subsequent oxidation for preparing hydrogen/tritium permeation barrier. International Journal of Hydrogen Energy 35(7): 2689-2693.
3. H Glasbrenner, A Perujo, E Serra (1995) Hydrogen Permeation Behavior of Hot-Dip Aluminized MANET Steel. Fusion Technology 28(3): 1159-1164.
4. ZG Zhang, YP Peng, YL Mao, CJ Pang, LY Lu (2012) Effect of hot-dip aluminizing on the oxidation resistance of Ti–6Al–4V alloy at high temperatures. Corrosion Science 55: 187-193.
5. SP Wang, L Zhou, CJ Li, ZX Li, HZ Li, et al. (2020) Morphology of composite coatings formed on Mo1 substrate using hot-dip aluminizing and micro-arc oxidation techniques. Applied Surface Science 508: 144761.
6. T Yener (2019) Chromium-Aluminide Coatings via Pack Cementation Method on Inconel 718 Alloy and Fe-Cr-Ni Super Alloy. Sakarya University Journal of Science 23: 817-823.
7. T Yener (2019) Low temperature aluminizing of Fe-Cr-Ni super alloy by pack cementation. Vacuum 162(6): 114-120.
8. S Mozgovoy, L Alik, J Hardell, B Prakash (2019) Material transfer during high temperature sliding of Al-Si coated 22MnB5 steel against PVD coatings with and without aluminium. Wear 426-427: 401-411.
9. K Bobzin, T Brögelmann, C Kalscheuer, T Liang (2019) Post-annealing of (Ti,Al,Si)N coatings deposited by high speed physical vapor deposition (HS-PVD). Surface and Coatings Technology 375: 752-762.
10. C Ye, L Jia, G Xu, F Wang, X Wang, et al. (2019) Microstructure and initial corrosion behavior of double-layer Zn-Al-Mg coatings produced by PVD. Surface and Coatings Technology 366: 214-226.
11. J Wagner, V Edlmayr, M Penoy, C Michotte, C Mitterer, et al. (2008) Deposition of Ti-Al-N coatings by thermal CVD. International Journal of Refractory Metals and Hard Materials 26(6): 563-568.
12. T Ishigaki, S Tatsuoka, K Sato, K Yanagisawa, K Yamaguchi (2018) Influence of the Al content on mechanical properties of CVD aluminum titanium nitride coatings. International Journal of Refractory Metals and Hard Materials 71: 227-231.
13. SI Castañeda, FJ Pérez (2018) Al-Mn CVD-FBR coating on P92 steel as protection against steam oxidation at 650 °C: TGA-MS study. Journal of Nuclear Materials 499: 419-430.
14. G CelebiEfe, M İpek, C Bindal, S Zeytin (2017) Pack Siliconizing of Ti6Al4V Alloy. Acta Physica Polonica A 132(3): 760-762.
15. T Yener, KM Doleker, A Erdogan (2019) High temperature oxidation behavior of low temperature aluminized Mirrax® ESR steel. Materials Research Express 6(11).
16. J Wang, DJ Wu, CY Zhu, ZD Xiang (2013) Low temperature pack aluminising kinetics of nickel electroplated on creep resistant ferritic steel. Surface and Coatings Technology 236: 135-141.
17. T Yener, GÇ Efe, M İpek, S Zeytin (2019) Low temperature aluminising of Inconel718 alloy by pack cementation. Indian Journal of Chemical Technology 26: 244-247.
18. X Shi, TA Nguyen, Z Suo, J Wu, J Gong, et al. (2012) Electrochemical and mechanical properties of superhydrophobic aluminum substrates modified with nano-silica and fluorosilane. Surface & Coatings Technology 206(17): 3700-3713.
19. TT Lee, TV Nguyen, TA Nguyen, TTH Nguyen, H Thai, et al. (2019) Thermal, mechanical and antibacterial properties of water-based acrylic Polymer/SiO_2-Ag nanocomposite coating. Materials Chemistry and Physics 232: 362-366.
20. X Shi, TA Nguyen, Z Suo, Y Liu, R Avci (2009) Effect of nanoparticles on the anticorrosion and mechanical properties of epoxy coating. Surface and Coating Technology 204(3): 237-245.
21. TV Nguyen, TA Nguyen, TH Nguyen (2020) The Synergistic Effects of SiO_2 Nanoparticles and Organic Photo stabiliziers for Enhanced Weathering Resistance of Acrylic Polyurethane Coating. Journal of Composites Science 4: 23.
22. H Zhang, H Qin, Z Ren, J Zhao, X Hou, et al. (2017) Low- temperature nitriding of nanocrystalline Inconel 718 alloy. Surface &Coatings Technology 330: 10-16.
23. E Hosseini, VA Popovich (2019) A review of mechanical properties of additively manufactured Inconel 718. Additive Manufacturing 30: 100877.
24. HX Wang, Y Zhang, SF Yang, BY Liu (2014) Effects of slurry pack cementation temperature on microstructure and wear resistance of TiAl co-deposited coating on copper plated nickel layer. Trans Nonferrous Met Soc China 24: 449-454.
25. H Qi, M Azer, A Ritter (2009) Studies of standard heat treatment effects on microstructure and mechanical properties of laser net shape manufactured INCONEL 718. Metallurgical and Materials Transactions A: Physical Metallurgy and Materials Science 40: 2410-2422.
26. S Gribbin, J Bicknell, L Jorgensen, I Tsukrov, M Knezevic (2016) Low cycle fatigue behavior of direct metal laser sintered Inconel alloy 718. International Journal of Fatigue 93: 156-167.
27. Z Pan, Y Feng, TP Hung, YC Jiang, FC Hsu, et al. (2017) Heat affected zone in the laser-assisted milling of Inconel 718. Journal of Manufacturing Processes 30: 141-147.
28. S Kim, H Choi, J Lee, S Kim (2020) Room and elevated temperature fatigue crack propagation behavior of Inconel 718 alloy fabricated by laser powder bed fusion. International Journal of Fatigue 140: 105802.

29. XJ Lu, ZD Xiang (2017) Formation of chromium nitride coatings on carbon steels by pack cementation process. Surface and Coatings Technology 309: 994-1000.

30. K Fujiwara, Z Horita (2002) Measurement of intrinsic diffusion coefficients of Al and Ni in Ni3Al using Ni/NiAl diffusion couples. Acta Materialia 50(6): 1571-1579.

31. J Li, Y Wu, Y Pan, W Liu, J Guo (2007) Influence of fluorides on phase transition of α- Al2O3 formation. Ceramics International 33(6): 919-923.

32. TF An, HR Guan, XF Sun, ZQ Hu (2000) Effect of the θ-α-Al2O3 transformation in scales on the oxidation behavior of a nickel-base superalloy with an aluminide diffusion coating. Oxidation of Metals. 54(3): 301-316.

33. JA Haynes, BA Pint, WD Porter, IG Wright (2004) Comparison of thermal expansion and oxidation behavior of various high-temperature coating materials and superalloys. Materials at High Temperatures 21(2): 87-94.

34. JM Brossard, J Balmain, F Sanchette, G Bonnet (2005) High-temperature oxidation of an aluminized NiCr alloy formed by a magnetron-sputtered Al diffusion coating. Oxidation of Metals 64(1): 43-61.

35. H Alimadadi, C Kjartansdóttir, A Burrows, T Kasama, P Møller (2017) Nickel-aluminum diffusion: A study of evolution of microstructure and phase. Materials Characterization 130: 105-112.

36. KM Doleker (2020) The Examination of Microstructure and Thermal Oxidation Behavior of Laser-Remelted High-Velocity Oxygen Liquid Fuel Fe/Al Coating. Journal of Materials Engineering & Performance 29: 3220-3232.

37. YZ Liu, XB Hu, SJ Zheng, YL Zhu, H Wei, et al. (2015) Microstructural evolution of the interface between NiCrAlY coating and superalloy during isothermal oxidation. Materials and Design 80: 63-69.

38. Y Jia, S Zhu, Z Liu, L Yang, M Shen, et al. (2020) Effects of oxygen incorporation in low expansion Ni+CrAlYN nanocomposite coatings on the oxidation behavior. Corrosion Science 167(6): 108550.

39. S Rashidi, JP Choi, JW Stevenson, A Pandey, RK Gupta (2020) High temperature oxidation behavior of aluminized Haynes 230. Corrosion Science 174: 108835.

40. CJ Wang, SM Chen (2006) Microstructure and cyclic oxidation behavior of hot dip aluminized coating on Ni-base superalloy Inconel 718. Surface and Coatings Technology 201(7): 3862-3866.

41. PK Koech, CJ Wang (2018) High-Temperature Corrosion Behavior of Aluminized- Coated and Uncoated Alloy 718 Under Cyclic Oxidation and Corrosion in NaCl Vapour at 750 °C. Oxidation of Metals 90: 713-735.

ISSN: 2574-1241

DOI: 10.26717/BJSTR.2022.40.006504

L Castañeda. Biomed J Sci & Tech Res